Supplementary Information: Magnetic imaging under high pressure with a spin-based quantum sensor integrated in a van der Waals heterostructure

Z. Mu,[1] J. Fraunié,[2] A. Durand,[1] S. Clément,[1] A. Finco,[1] J. Rouquette,[3] A. Hadj-Azzem,[4] N. Rougemaille,[4] J. Coraux,[4] J. Li,[5] T. Poirier,[5] J. H. Edgar,[5] I. C. Gerber,[2] X. Marie,[2] B. Gil,[1] G. Cassabois,[1,6] C. Robert,[2] and V. Jacques[1]

[1] *Laboratoire Charles Coulomb, Université de Montpellier and CNRS, 34095 Montpellier, France*

[2] *Université de Toulouse, INSA-CNRS-UPS, LPCNO, 135 Avenue Rangueil, 31077 Toulouse, France*

[3] *Institut Charles Gerhardt, Université de Montpellier and CNRS, 34095 Montpellier Cedex, France*

[4] *Univ. Grenoble Alpes, CNRS, Grenoble INP, Institut NEEL, 38000 Grenoble, France*

[5] *Tim Taylor Department of Chemical Engineering, Kansas State University, Kansas 66506, USA*

[6] *Institut Universitaire de France, 75231 Paris, France*

Supplementary Note 1

All magnetic imaging experiments (Fig. 4 and Fig. 5) were performed with a bias magnetic field $B_b = 8$ mT applied along the z-axis in order to split the electron spin resonance of the V_B^- centers via the Zeeman effect. We then measured the frequency ν_- of the lower electron spin resonance at each point of the scan. Taking into account the orthorhombic zero-field splitting parameter E, this frequency is given by

$$\nu_- = D(P) - \sqrt{E^2 + \gamma_e^2 (B_b + B_z)^2} \ , \tag{1}$$

where $\gamma_e = 28$ GHz/T and B_z is the magnetic field produced by the $CrTe_2$ flake along the z direction, which is in the mT range in our experiments. For the hBN sensing layer used for magnetic imaging under pressure, the orthorhombic zero-field splitting parameter is $E = 60(2)$ MHz (see Supplementary Figure 3). The Zeeman term is therefore always much larger than the E parameter in magnetic imaging experiments and we can thus make the approximation $\sqrt{E^2 + \gamma_e^2 (B_b + B_z)^2} \sim \gamma_e (B_b + B_z)$. The relative error ($\sim 3\%$) introduced by this approximation in the magnetic field estimation is much smaller than that resulting from the pixel-to-pixel noise of the magnetic field images.

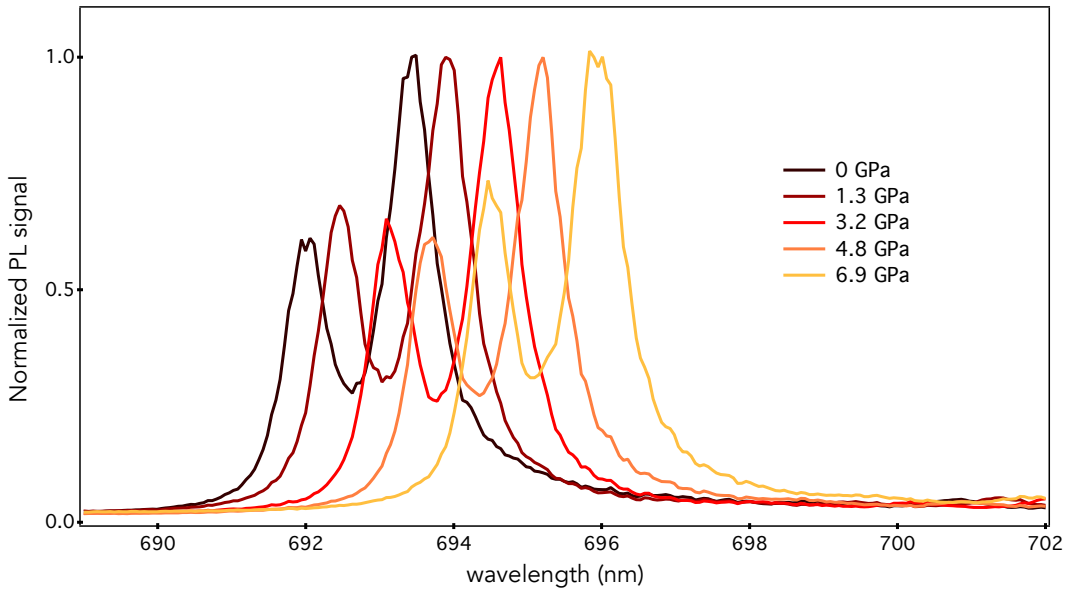

Supplementary Figure 1. Typical emission spectra of a ruby microcrystal loaded inside the high-pressure chamber of the DAC. The shift of the emission peaks is used to calibrate the pressure. The emission lines are not broadened in the considered pressure range, which indicates a quasi-hydrostatic pressure environment. For these measurements, NaCl was used as pressure transmission medium. Similar results were obtained for Daphne oil 7373.

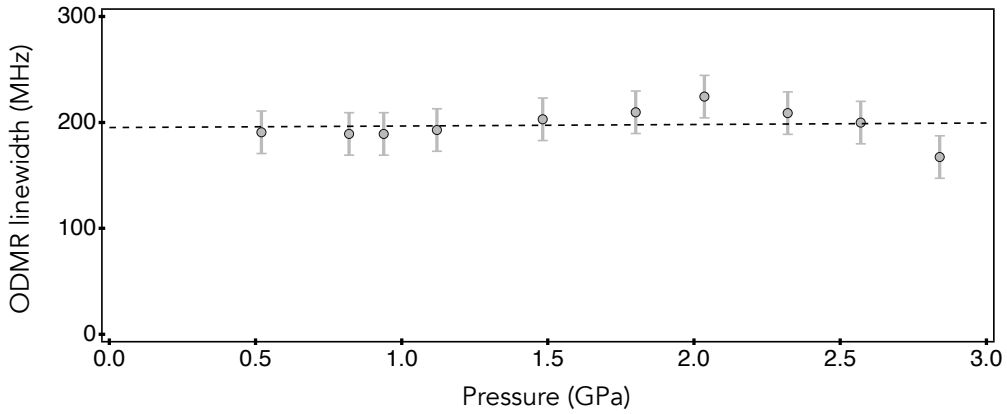

Supplementary Figure 2. Pressure-dependent ODMR linewidth (FWHM) obtained for the set of data used in Figure 3 of the main manuscript. The error bars correspond to one standard error in the fitting of ODMR spectra with Lorentzian functions.

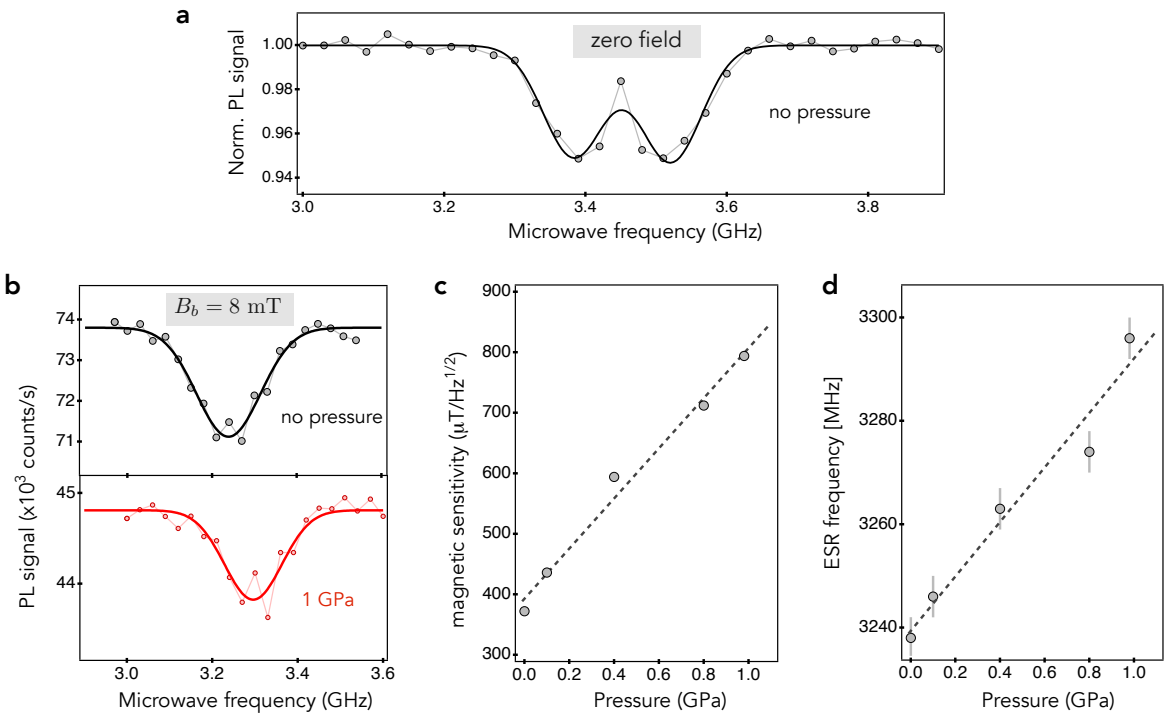

Supplementary Figure 3. Characterization of the hBN sensing layer used for magnetic imaging of micrometer-sized $CrTe_2$ flakes.(a) Typical ODMR spectrum recorded at zero magnetic field from a hBN flake used for magnetic imaging experiment. This flake was exfoliated from a bulk hBN crystal isotopically purified with ^{15}N, which has been irradiated by thermal neutrons with a dose of $\sim 1.4 \times 10^{17}$ neutrons/cm^2 (see Methods). Data fitting with Gaussian functions leads to an orthorhombic splitting $E = 60(2)$ MHz. This value is smaller than that shown in Figure 2 of the main manuscript ($E \sim 100$ MHz), which was obtained from measurements performed on another hBN crystal irradiated with a higher neutron dose ($\sim 2.6 \times 10^{17}$ neutrons/cm^2). (b) Spectra of the low-frequency magnetic resonance (ν_-) of the V_B^- center recorded far from the $CrTe_2$ flake at two different pressures with a bias field $B_b = 8$ mT. The solid lines are data fitting with a Gaussian function. (c) Magnetic field sensitivity as a function pressure. (d) Magnetic resonance frequency ν_- as a function of pressure. The black dashed line is a linear fit of the data from which we extract $\alpha = 52 \pm 6$ MHz/GPa. The error bars correspond to one standard error in the fitting of ODMR spectra with a Gaussian function.

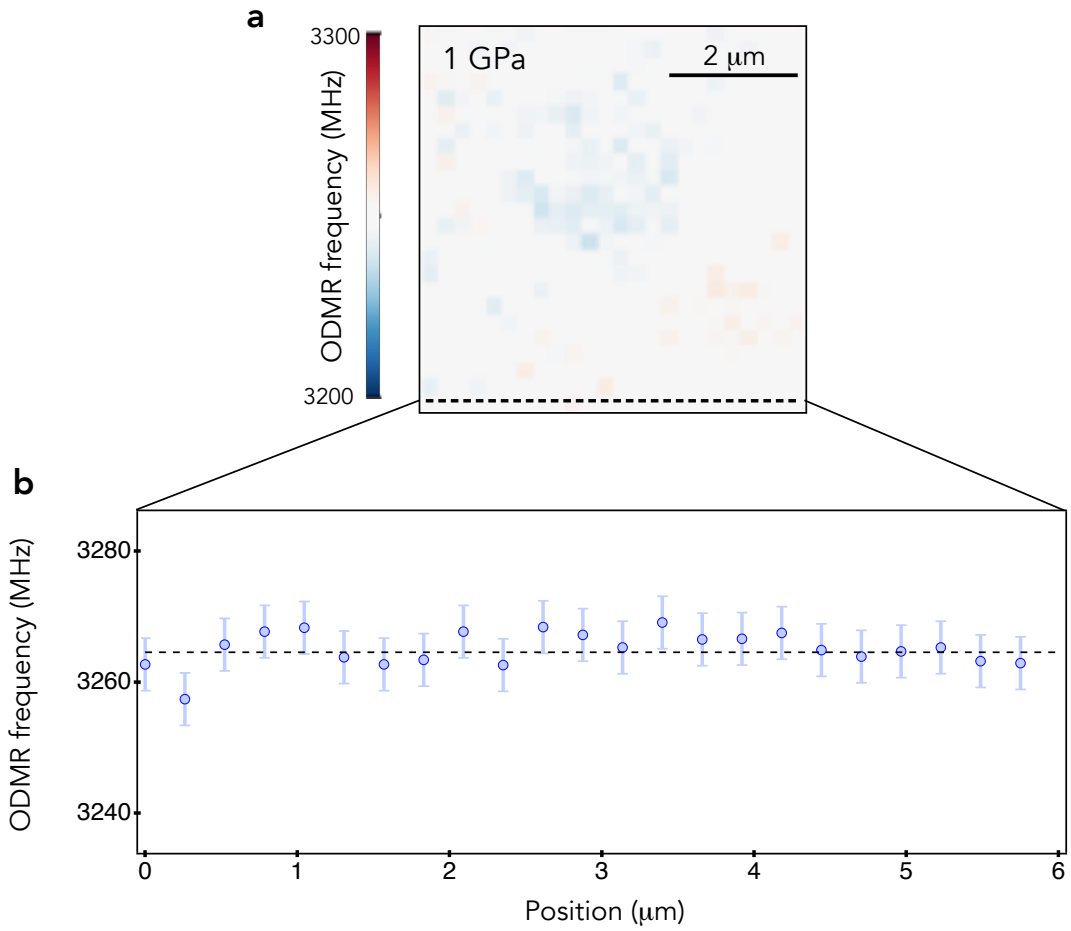

Supplementary Figure 4. (a) Map of the ODMR frequency recorded at 1 GPa for the second hBN/$CrTe_2$/hBN heterostructure. This map corresponds to that shown in Figure 5c of the main text. (b) Linecut of the ODMR map along the black dashed line in (a), showing a typical variation of the ODMR frequency by $\sim$ 5 MHz that corresponds to the pixel-to-pixel noise in our images. We can thus conclude that our measurements do not reveal a significant spatial gradient of the in-plane stress component on a length scale of about 5 μm. The error bars correspond to one standard error in the fitting of ODMR spectra.

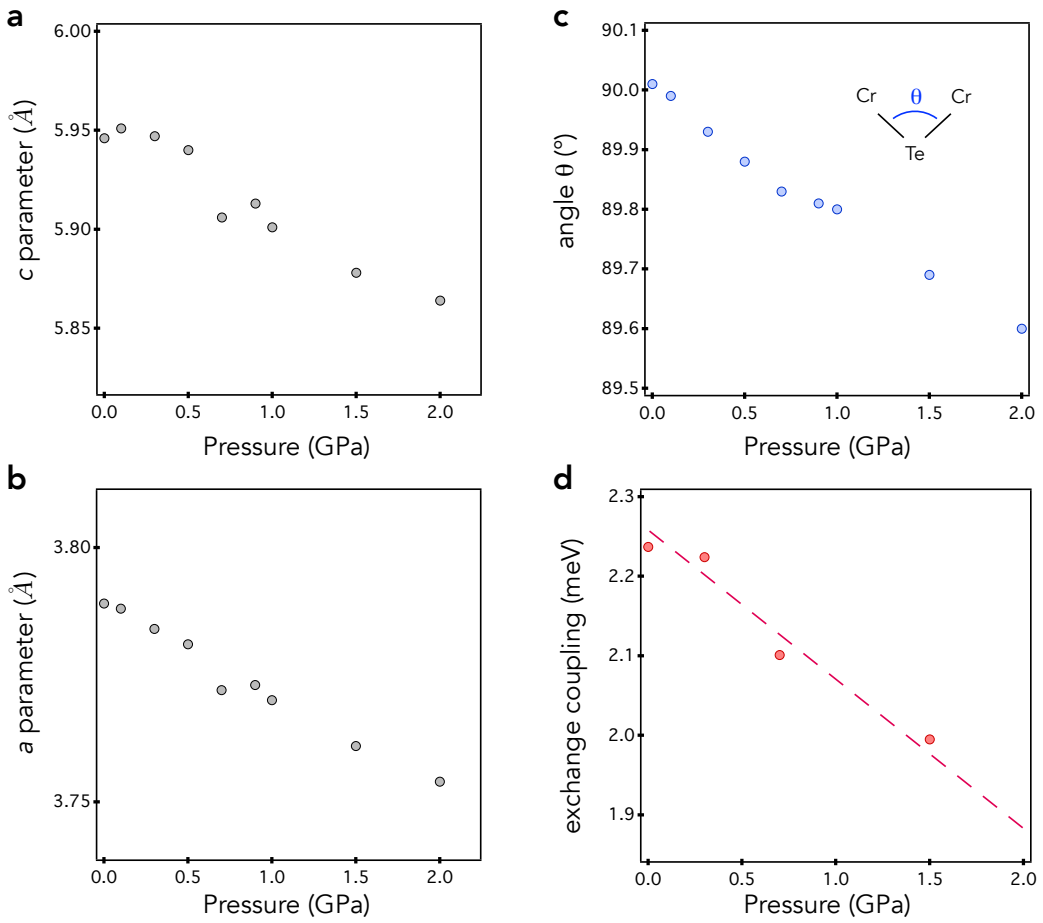

Supplementary Figure 5. Results of first-principles calculations. (a,b) Lattice constants c (top panel) and a (bottom panel) of $CrTe_2$ as a function of pressure. (c) Evolution of the Cr-Te-Cr bound angle θ with pressure. (d) Effective exchange coupling parameter as a function of pressure.